

# MAPF-World: Action World Model for Multi-Agent Path Finding

Zhanjiang Yang<sup>1</sup>, Yang Shen<sup>2</sup>, Yueming Li<sup>1</sup>, Meng Li<sup>†1</sup>, Lijun Sun<sup>†1</sup>

**Abstract**—Multi-agent path finding (MAPF) is the problem of planning conflict-free paths from the designated start locations to goal positions for multiple agents. It underlies a variety of real-world tasks, including multi-robot coordination, robot-assisted logistics, and social navigation. Recent decentralized learnable solvers have shown great promise for large-scale MAPF, especially when leveraging foundation models and large datasets. However, these agents are reactive policy models and exhibit limited modeling of environmental temporal dynamics and inter-agent dependencies, resulting in performance degradation in complex, long-term planning scenarios. To address these limitations, we propose MAPF-World, an autoregressive action world model for MAPF that unifies situation understanding and action generation, guiding decisions beyond immediate local observations. It improves situational awareness by explicitly modeling environmental dynamics, including spatial features and temporal dependencies, through future state and actions prediction. By incorporating these predicted futures, MAPF-World enables more informed, coordinated, and far-sighted decision-making, especially in complex multi-agent settings. Furthermore, we augment MAPF benchmarks by introducing an automatic map generator grounded in real-world scenarios, capturing practical map layouts for training and evaluating MAPF solvers. Extensive experiments demonstrate that MAPF-World outperforms state-of-the-art learnable solvers, showcasing superior zero-shot generalization to out-of-distribution cases. Notably, MAPF-World is trained with a 96.5% smaller model size and 92% reduced data. The source code will be available upon paper acceptance.

**Index Terms**—Multi-agent path finding, action world model, decentralized decision-making, real-world map

## I. INTRODUCTION

Multi-agent path finding (MAPF) [1] is a fundamental problem in robotics and embodied intelligence, with applications in autonomous driving, collective robotics, warehouse automation, etc [2]. The problem is known to be NP-hard [3]–[6], presenting significant challenges due to strict conflict-free constraints on path planning, especially in large-scale scenarios with many agents and complex layouts under real-time requirements. Moreover, prevailing artificial benchmark maps often limit the generalizability of MAPF solvers, as these maps may fail to capture the topological complexity of real-world environments.

Classical centralized and heuristic-based methods, such as CBS [7] and PBS [8], provide (sub-)optimal solutions but struggle with scalability. To address this, PIBT [9] offers a

heuristic online approach with compromised solution quality, while LaCAM\* [10], [11] presents an anytime near-optimal method that excels in efficiency. As emerging solutions, decentralized learning-based methods primarily leverage imitation learning (IL) and reinforcement learning (RL), enhancing performance by incorporating additional information through communication, centralized collision resolution, and global guidance, as seen in SCRIMP [12] and SILLM [13]. More recent learnable solvers push the frontier further by utilizing large datasets, foundation models, and fine-tuning techniques, such as MAPF-GPT [14] and MAPF-GPT-DDG [15]. However, these methods design reactive policy models that produce actions solely based on current observations, potentially failing to capture the complexity of large, intricate environmental layouts and temporal dynamics of crowded agents, which can lead to performance degradation in complex, long-term planning scenarios with partial observation.

To overcome the above limitations of the reactive policies, we propose **MAPF-World**, an autoregressive **action world model** for MAPF inspired by Kahneman’s fast-slow dual-system theory [16]. As an action world model, MAPF-World integrates a policy (fast system) and a world model (slow system) within a unified Transformer architecture. This framework utilizes a shared encoder and dual-branch decoders, with a fast head for rapid policy decisions and a slow head for future state prediction. By learning the world model and action policy together with the injection of action generation capability, our end-to-end approach enables the model to learn more complex, high-level planning strategies. The main advantage of MAPF-World is that it enhances situational awareness and contextual reasoning by explicitly modeling environmental dynamics, including spatial features, temporal dynamics, and multi-agent dependencies, through the supervised prediction of future states and actions. Incorporating these predicted futures allows MAPF-World to make more informed, coordinated, and far-sighted decisions in an autoregressive manner, particularly in complex multi-agent settings on large maps.

In summary, our main **contributions** are as follows.

- We present an automated pipeline that generates realistic MAPF maps from urban layouts, bridging the gap between synthetic benchmarks and real-world applications.
- We propose MAPF-World, an autoregressive action world model for MAPF that utilizes future predictions to guide current decision-making in complex multi-agent settings.
- We conduct extensive empirical studies, demonstrating the superior performance of MAPF-World, particularly in high-density and large-scale scenarios, with a signifi-

\* Equal contribution.

† Corresponding author.

<sup>1</sup> Shenzhen Technology University, China. (2410263030@mails.sztu.edu.cn, 202301510025@stumail.sztu.edu.cn, \{limeng2, sunlijun\}@sztu.edu.cn)

<sup>2</sup> University of Technology Sydney, Australia. (Yang.Shen-9@student.uts.edu.au)

antly more compact model and less training data.

## II. RELATED WORK

*Benchmarks:* A problem instance is defined by three components: a map, a set of agents, and their start and goal positions. Existing benchmark maps [1], [17], [18] are generally grouped by topologies, including empty, random, mazes, rooms<sup>12</sup>, warehouses<sup>2</sup> (12 maps), terrains<sup>1</sup> (20 maps), video games<sup>1</sup> (454 maps), and city streets<sup>12</sup> (90 maps for 10 cities). Recent works also investigate optimizing map layouts [19] and generating map patterns by neural cellular automata [20], [21]. POGEMA [18] includes a problem instance generator for random, mazes, and warehouse maps. However, real-world maps, such as those from city data, are relatively scarce, limiting the evaluation of solver’s generalizability to practical scenarios. Our work helps bridge the gap by introducing a pipeline to generate maps from real-world city data.

*MAPF Solvers:* Classical MAPF solvers are typically search-based. Heuristic methods like CBS [7], PBS [8], WHCA\* [22] provide (sub)optimal solutions but struggle with scalability issues. To address this, state-of-the-art anytime planners such as LaCAM\* [10], [11] improve efficiency, offering a trade-off between speed and solution quality. In contrast, learning-based methods offer scalable, efficient, and suboptimal solutions, primarily based on imitation learning (IL) and reinforcement learning (RL). These methods are generally categorized into hybrid and end-to-end approaches. Hybrid approaches replace partial components in heuristic algorithms with learnable modules. For example, LNS2+RL [23] replaces the prioritized planning (PP) module with an RL strategy for improved sub-solution selection in LNS2. The second category relies entirely on end-to-end learning. For example, SCRIMP [12] uses MARL for communication and priority assignment to tackle challenges from agents’ limited field of view, while MAPF-GPT [14] introduces an 85M foundation model trained with IL on a 1B expert dataset, outperforming existing RL-based solvers. MAPF-GPT-DDG [15] further improves MAPF-GPT via fine-tuning on difficult instances. All these existing methods are primarily reactive. Our work, MAPF-World, takes a different approach by introducing an action world model to enable more far-sighted planning.

*Action World Model and Fast-Slow Dual-System:* A world model [24], [25] is a generative model that predicts future states from current observations. It has made significant strides in artificial general intelligence (AGI) [26]–[30]. With foundation models trained on large-scale data [31], world model learning for decision making has made significant strides in artificial general intelligence (AGI) [26]–[30]. Recently, the concept of action world model has been further introduced in WorldVLA [32], which extends traditional world models by integrating action generation into the world modeling and observation/action understanding into the action model. However, despite being an action world model, our proposed MAPF-World is built on Kahneman’s fast-slow dual-system [16],

akin to LeCun’s two-mode architecture for the observation-action loop [33]. Moreover, MAPF-World embeds the fast system in the slow system by sharing parameters, similar to the Fast-in-Slow (FiS) dual-system vision-language-action (VLA) model [34]. However, a key distinction is that MAPF-World operates as a complete action world model, capable of autoregressively predicting the entire next state and multi-agent interactions required for multi-step planning.

## III. BACKGROUND

*Multi-agent path finding (MAPF).* The MAPF problem is defined on a 2-D grid map with a set of agents  $\mathcal{I} = \{1, \dots, n\}$ . Each agent  $i \in \mathcal{I}$  is assigned a start position  $s_i \in \mathcal{S}$  and a goal position  $g_i \in \mathcal{S}$ , where  $\mathcal{S}$  denotes the set of all free cells. At each discrete time step, agent  $i$  selects an action  $a_i \in \{\text{Up, Right, Down, Left, Wait}\}$ , and the joint action  $\mathbf{a} = \{a_1, \dots, a_n\}$  updates the system state. A solution is a set of collision-free paths  $\{\tau_i\}_{i \in \mathcal{I}}$ , where each  $\tau_i = (s_i^0, s_i^1, \dots, g_i)$  is a sequence of positions from start to goal. Two types of collisions are forbidden, which are vertex collision and edge collision [1]. For learning-based MAPF solvers, *success rate* is the most commonly used objective function.

*Decentralized Partially Observable Markov Decision Process (Dec-POMDP).* A Dec-POMDP is a multi-agent sequential decision-making problem under the Markov assumption, which is constrained by decentralized decision and partial observation. It can be defined as  $\langle \mathcal{I}, \mathcal{S}, \mathcal{A}, \mathcal{O}, P, O \rangle$ .  $\mathcal{I} = \{1, \dots, n\}$  is the set of all agents.  $\mathcal{S} = \{(x_i, y_i) | i \in \mathcal{I}\}$  is the true state space, i.e., the 2-D positions of all agents in MAPF.  $\mathcal{A} = A_1 \times \dots \times A_n = \{\mathbf{a}\} = \{a_i(s) | i \in \mathcal{I}\}$  is the joint action space, where  $a_i = \{0, 1, \dots, 4\}$  represents moving up, right, down, left, and waiting.  $\mathcal{O} = O_1 \times \dots \times O_n$  is the joint observation space. The transition function  $P(s'|s, \mathbf{a})$  represents the probability of the system moving from the current state  $s$  to the next state  $s'$  given the joint action  $\mathbf{a}$ .  $O = \{o_i(s) | i \in \mathcal{I}\}$  is the joint observation function.

*Action World Model.* An agent  $i$  is an action world model, which has two functional components in one unified framework: a policy model  $\pi_i$  and a world model  $f_i$ . A policy model  $\pi_i(a_t | o_{t-h:t}; \theta)$  makes a reactive action  $a_t$  decision to historical observations  $o_{t-h:t}$ . A world model  $f_i(o_{t+1} | o_{t-h:t}, a_{t-h:t}; \phi)$  is a generative model that captures the dynamics of an environment by predicting the future state  $o_{t+1}$  from past observations  $o_{t-h:t}$  and actions  $a_{t-h:t}$ . These two models are learned together by minimizing  $\min_{\theta, \phi} E_{s_t \sim P(o_t | o_{t-1}, \mathbf{a}_{t-1})} [\lambda_1 \cdot L_{\pi_i} + \lambda_2 \cdot L_{f_i}]$ , where  $L_{\pi_i}$  and  $L_{f_i}$  are the losses for  $\pi_i$  and  $f_i$ , respectively, while  $\lambda_1$  and  $\lambda_2$  are two constants.

## IV. METHOD

### A. Overview

In this section, we propose MAPF-World, an autoregressive action world model for MAPF that integrates action generation and world understanding, as shown in Fig. 1. MAPF-World is designed as a fast-slow dual-system based on the Transformer architecture, which embeds the fast system within the slow

<sup>1</sup><https://movingai.com/benchmarks/grids.html>

<sup>2</sup><https://movingai.com/benchmarks/mapf.html>

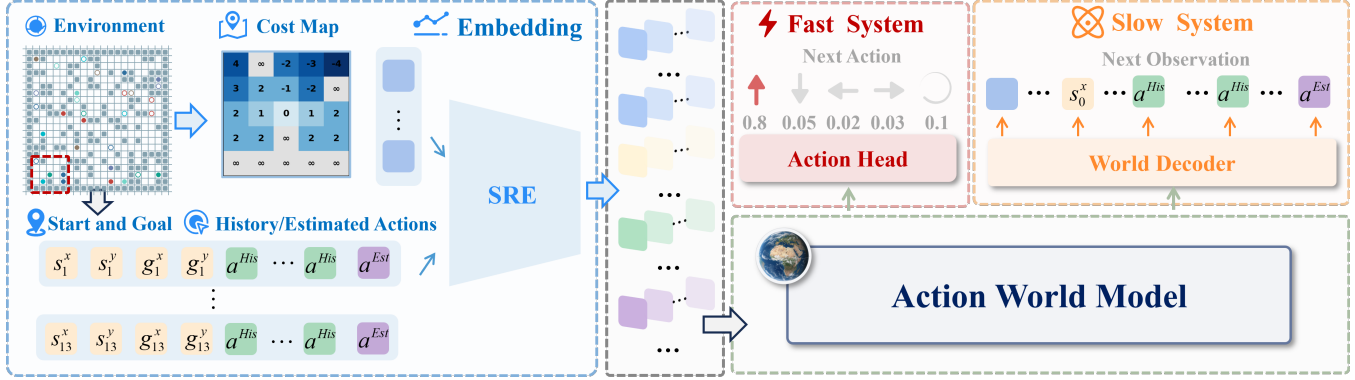


Fig. 1: Overview of the proposed **MAPF-World**, an autoregressive action world model based on fast-slow dual system. It encodes local cost maps and information about neighboring agents. Spatial Relational Encoding (SRE) is used to strengthen agent-map and agent-agent associations as input. The Action World model uses the Fast system for rapid policy decisions and the Slow system for future state and interaction predictions.

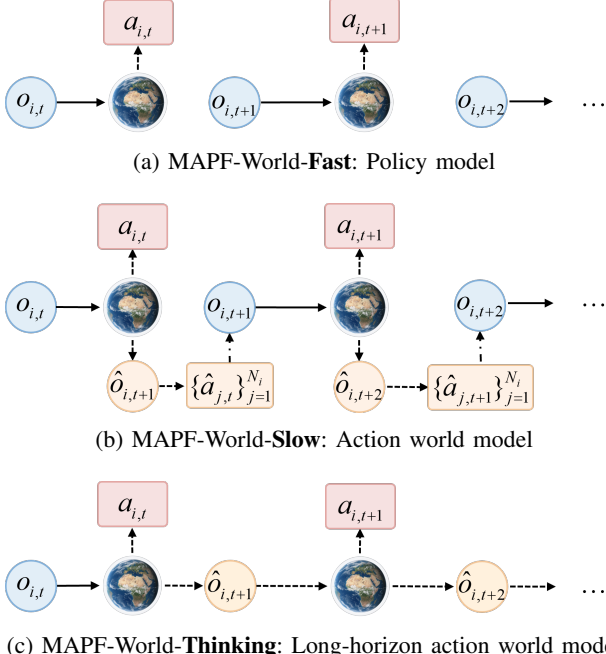


Fig. 2: Three work modes of MAPF-World. (Solid arrows: real observations; dashed arrows: predictions.)

system with a shared encoder and dual-branch decoders. The **fast system** (action head) generates the agent’s next action, while the **slow system** (world head) predicts the next environmental observation and actions of itself and other agents. In particular, MAPF-World works in one of three modes shown in Fig. 2, allowing for a trade-off between reactivity and long-horizon planning:

- **MAPF-World-Fast (Policy model):** The fast system, i.e., the policy model, takes the current observation  $o_t$  as input, outputs the next action  $a_t$ , and executes it (Fig. 2a).
- **MAPF-World-Slow (Action world model):** The slow system, i.e., the action world model, works autoregressively.

It takes the observation  $o_t$  as input, and predicts its own action  $a_t$  and next observation  $\hat{o}_{i,t+1}$ , which includes predicted actions of neighboring agents  $\{\hat{a}_{j,t}\}_{j=1}^{N_i}$ . These predicted actions  $\{\hat{a}_{j,t}\}_{j=1}^{N_i}$  are then fed into the input observation at the next time step  $o_{t+1}$ . This allows the model to incorporate predicted information of other agents, enabling more coordinated decision-making (Fig. 2b).

- **MAPF-World-Thinking (Long-horizon action world model):** The slow system, i.e., the action world model, works autoregressively over a larger horizon  $H$ . Every  $H$  steps, the first step uses the real observation  $o_t$  to predict  $a_t$  and  $o_{t+1}$ , executes  $a_t$ , and then plans and acts based on predictions for the next  $H - 1$  steps (Fig. 2c).

#### B. Spatial Relational Encoding (SRE)

We adopt the tokenizer and observation organization used by MAPF-GPT [14]. The input of the model includes a local cost map and per-agent state information (i.e., relative positions and goal locations, action history, estimated actions). The input consists of 256 tokens with 121 tokens (11×11 field of view) for the cost map, and 135 tokens (10 tokens for a maximum of 13 agents) for the agent information. A key challenge is injecting spatial awareness and agent-level semantic information into the encoder. Conventional position encodings, which assign embeddings based on token index, fail to capture agent-level semantics and relative motion intent. We address this by proposing the Spatial Relational Encoding (SRE) scheme that aligns the contextual guidance from the local cost map with the semantic states in agent-level tokens.

*Polar Coordinate Encoding:* First, a Euclidean coordinate  $(x, y)$  is mapped to a polar representation by  $\text{Polar}(x, y) = [r, \sin \theta, \cos \theta]$ , where  $r = \sqrt{x^2 + y^2}$ , and  $\theta = \arctan 2(y, x)$ . This 3D vector captures both distance and direction information. Then a shared linear layer  $\text{Linear}: \mathbb{R}^3 \rightarrow \mathbb{R}^d$  is applied to all polar vectors to match the model’s hidden dimension  $d$ .

*Agent-Level Position Encoding:* For each agent  $i$ , we define the goal displacement vector based on its start position  $s_i =$



Fig. 3: Examples ( $256 \times 256$ ) of real-world map generator presented in Section IV-D.

$(x_i^s, y_i^s)$  and goal position  $\mathbf{g}_i = (x_i^g, y_i^g)$  in the token sequence:

$$\Delta \mathbf{p}_i = \mathbf{g}_i - \mathbf{s}_i. \quad (1)$$

Then, the position encoding for the 10-token segment of agent  $i$  is defined by three types of embeddings:

$$\mathbf{e}_i = (\mathbf{e}_i^s, \mathbf{e}_i^s, \mathbf{e}_i^g, \mathbf{e}_i^g, \underbrace{\mathbf{e}_i^\Delta, \dots, \mathbf{e}_i^\Delta}_{\text{repeat 6 times}}) \in \mathbb{R}^{10 \times d} \quad (2)$$

where  $\mathbf{e}_i^s = \text{Linear}(\text{Polar}(\mathbf{s}_i))$  encodes the start position,  $\mathbf{e}_i^g = \text{Linear}(\text{Polar}(\mathbf{g}_i))$  encodes the goal position, and  $\mathbf{e}_i^\Delta = \text{Linear}(\text{Polar}(\Delta \mathbf{p}_i))$  represents the displacement.

This decomposition enables the model to explicitly distinguish between static spatial context (start/goal) and dynamic intent (displacement), enabling more semantic attention allocation.

*Cost Map Position Encoding:* For the 121 cost map tokens, the positional encoding of a token is defined by its fixed spatial position  $(x, y)$  on the  $11 \times 11$  egocentric local map:

$$\mathbf{e}_{(x,y)}^{\text{map}} = \text{Linear}(\text{Polar}(x, y)) \in \mathbb{R}^d. \quad (3)$$

*Combined Position Encoding:* The final position encoding for the 256 tokens is the concatenation of the cost map and  $N_i$  ( $N_i \leq 13$ ) neighboring agents' information:

$$\mathbf{E}_{\text{SRE}} = \text{Concat}(\mathbf{e}_{(x,y)}^{\text{map}}, \{\mathbf{e}_i\}_{i=1}^{N_i}, \mathbf{0}^{5 \times d}) \in \mathbb{R}^{256 \times d}. \quad (4)$$

This position embedding is then added to the token embedding  $\mathbf{E}_{\text{Token}}$  before being fed into the Transformer encoder, yielding

$$\mathbf{X} = \mathbf{E}_{\text{Token}} + \mathbf{E}_{\text{SRE}} \in \mathbb{R}^{256 \times d}. \quad (5)$$

### C. Model Training

The fast and slow systems are trained jointly using the cross-entropy (CE) loss. For each token position  $k$ , the loss for the  $b$ -th sample is:

$$\mathcal{L}^{(b,k)} = -\log(\hat{y}_{b,k}[Y_{b,k}]) \quad (6)$$

where  $\hat{y}_{b,k}$  and  $Y_{b,k}$  are the corresponding predicted probability distribution and true label (an index), respectively.

Then, the loss for the slow system is:

$$\mathcal{L}_{\text{slow}} = \frac{1}{B \sum_{k=1}^T w_k} \sum_{b=1}^B \sum_{k=1}^T w_k \cdot \mathcal{L}^{(b,k)} \quad (7)$$

where  $B$  is the batch size, and

$$w_k = \begin{cases} 0.5 & \text{if } k < 121 \\ 0.0 & \text{if } k \in \mathcal{M} \\ 1.0 & \text{if } k \in \mathcal{A} \cup \mathcal{G} \\ 0.5 & \text{otherwise} \end{cases} \quad (8)$$

with

- $\mathcal{M}$ : The set of token positions that are masked;
- $\mathcal{A}$ : The set of token positions for real action;
- $\mathcal{G}$ : The set of token positions for estimated action.

We assign larger weights to action-related tokens to prioritize accurate action prediction, as these directly influence downstream planning performance.

The fast system is dedicated solely to supervising the agent's own next action, so the first 255 tokens are masked out (set as -1), and the last token position outputs the action. Therefore, the loss for the fast system is:

$$\mathcal{L}_{\text{fast}} = \frac{1}{B} \sum_{b=1}^B \mathcal{L}^{(b,256)} \quad (9)$$

Finally, the total loss for the fast-slow dual system is:

$$\mathcal{L} = \mathcal{L}_{\text{fast}} + 0.5\mathcal{L}_{\text{slow}}. \quad (10)$$

### D. Real-World Map Generator

To bridge the gap between benchmarks and real-world applications, we propose a pipeline that automatically generates grid-based maps for MAPF from real-world urban layouts. The pipeline uses OpenStreetMap (OSM)<sup>3</sup> tags to identify walkable areas (e.g., footway, path, residential, pedestrian), while building footprints, natural barriers, and other non-navigable land use areas are marked as obstacles. Additionally, the pipeline supports batch processing for large geographical regions. In this work, we use this pipeline to generate 137 maps from 11 European cities with a size of  $256 \times 256$ .

Specifically, the spatial region of interest is rasterized into grids with each cell corresponding to a user-defined resolution (e.g., 1 meter per cell). Post-processing steps are then applied, including morphological operations to eliminate noise (e.g., narrow gaps, isolated pixels) and optional boundary smoothing to improve grid structure quality. The resulting maps preserve the structural and topological characteristics of real cities, supporting both dense urban and sparse suburban areas.

## V. EXPERIMENT

### A. Datasets

For training, we generate the expert dataset using the pipeline provided by MAPF-GPT [14]. Specifically, we employ LaCAM\* [11] to solve 300K problem instances (8% of the total 3.75M instances in MAPF-GPT) on random

<sup>3</sup><https://www.openstreetmap.org/copyright>

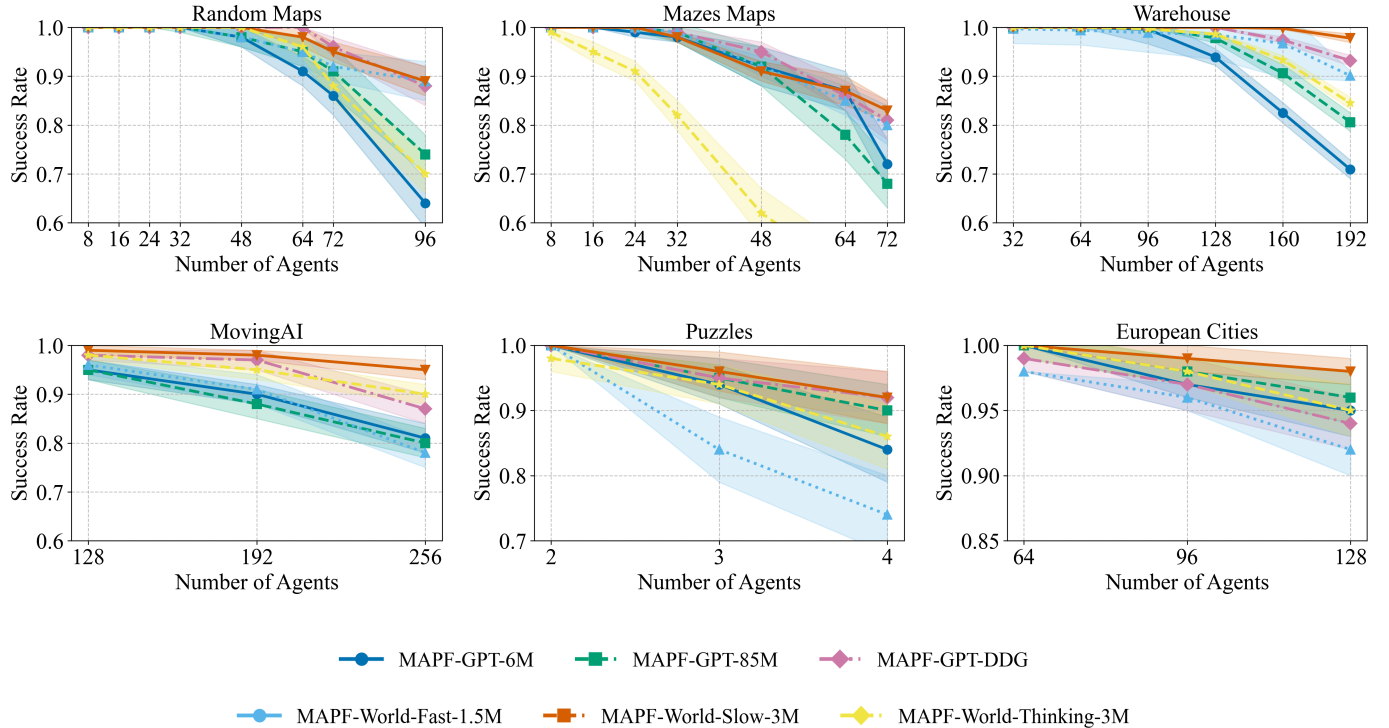


Fig. 4: Success rates of MAPF solvers on different benchmarking maps (higher is better).

and mazes maps, each with a 10-second time limit. These solutions are then processed into the 2-step observation–action tuple of the format  $(o_{t-1}, o_t, a_t)$  to train our action world model, in contrast to the single observation-action pair  $(o_t, a_t)$  used in the imitation learning of policy models (e.g., MAPF-GPT, MAPF-GPT-DDG [15]). Furthermore, we retain “wait-at-target” actions instead of discarding them like MAPF-GPT, as they are integral to the planning sequences and crucial for long-term planning. Finally, this process yields 80M training samples (40M each from random and mazes maps), a dataset **92% smaller** than the 1B samples used by MAPF-GPT.

### B. Evaluation

For evaluation, we compare MAPF solvers across six types of maps: random, mazes, warehouse, puzzles, MovingAI, and European city maps, as shown in Table I. The first five types are integrated in POGEMA [18]. European city maps are generated using our proposed map generator, examples of which are shown in Fig. 3. Success rate (SR) is the most commonly used metric by learning-based MAPF solvers, which is the rate of problem instances that are successfully solved within the given time steps or computation time.

### C. Baselines

Our proposed model MAPF-World has three work modes: MAPF-World-Fast, MAPF-World-Slow, and MAPF-World-Thinking. We conduct a comparative analysis against several state-of-the-art (SOTA) learning-based solvers and include ablations of our proposed model.

TABLE I: Details of datasets used in evaluation.

Dataset	Agents	Maps	Map Size	Seeds	Steps
Random	8, 16, ..., 72, 96	128	17×17, 21×21	1	128
Mazes	8, 16, ..., 64, 72	128	17×17, 21×21	1	128
Warehouse	32, 64, ..., 160, 192	1	33×46	128	128
MovingAI	128, 192, 256	128	64×64	1	256
Puzzles	2, 3, 4	16	5×5	10	128
European	64, 96, 128	137	60×60	1	128

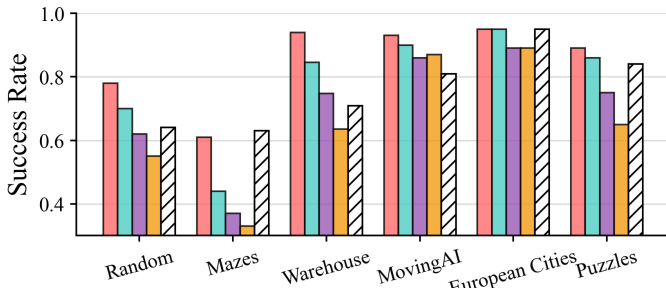
- MAPF-GPT-85M [14]: a large foundation model for MAPF with 85M parameters trained on a 1B expert dataset via imitation learning.
- MAPF-GPT-6M [14]: a compact version of MAPF-GPT with 6M parameters, trained on a reduced 150M sample dataset.
- MAPF-GPT-DDG [15]: a SOTA MAPF solver based on a fine-tuned MAPF-GPT-2M model, reported to surpass all contemporary learnable solvers.
- MAPF-World-Fast (ours): a policy model utilizes only the fast system of MAPF-World, with 1.5M parameters trained on an 80M dataset.
- MAPF-World-Slow (ours): an action world model uses the slow system of MAPF-World, with 2.7M parameters trained on an 80M dataset.
- MAPF-World-Thinking (ours): a long-horizon action world model, same as MAPF-World-Slow but works differently, enabling predictive, far-sighted planning.

Generating 80M expert dataset takes about two days on a workstation with 16 CPU cores. Training MAPF-World takes

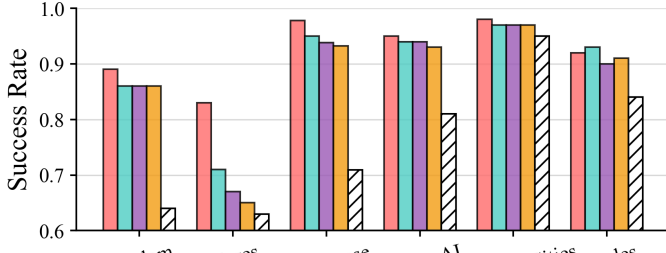
48 hours on a server with 1 NVIDIA V100 GPU and 64 CPU cores. All baselines are trained solely on synthetic benchmarks and have not seen real-world maps in training.

#### D. Main Results

*Fast vs. Slow System.* A direct comparison between our model’s components reveals the significant advantage of predictive planning. As shown in Fig. 4, MAPF-World-Slow (action world model) consistently outperforms MAPF-World-Fast (policy model) across nearly all test cases. Their performance gap is most pronounced in complex scenarios, such as the MovingAI, puzzles, and European city maps. Notably, the simpler MAPF-World-Fast remains competitive in low-density settings (e.g., random and warehouse maps) or on maps with intricate but locally navigable layouts (e.g., mazes). These results highlight the superior situational awareness conferred by the slow system’s world understanding and action generation, while also confirming the utility of the fast system in less congested scenarios.



(a) MAPF-World-Thinking



(b) MAPF-World-Slow

Legend: 2-steps (red), 3-steps (teal), 4-steps (purple), 5-steps (orange), MAPF-GPT-6M (diagonal lines).

Fig. 5: Ablation on MAPF-World’s thinking capability.

*Ours vs. SOTA Baselines.* We compare the MAPF-World-Fast and MAPF-World-Slow with SOTA policy models for MAPF, including MAPF-GPT-6M, MAPF-GPT-85M, and MAPF-GPT-DDG. The results in Fig. 4 demonstrate that MAPF-World-Slow consistently outperforms the strongest baseline, MAPF-GPT-DDG, on four of six map types (warehouse, MovingAI, puzzles, and European cities). Furthermore, it shows superior performance in high agent density scenarios

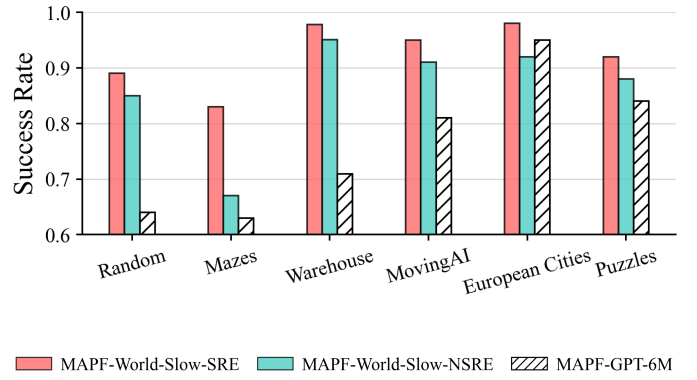


Fig. 6: Ablation on impact of spatial relational encoding.

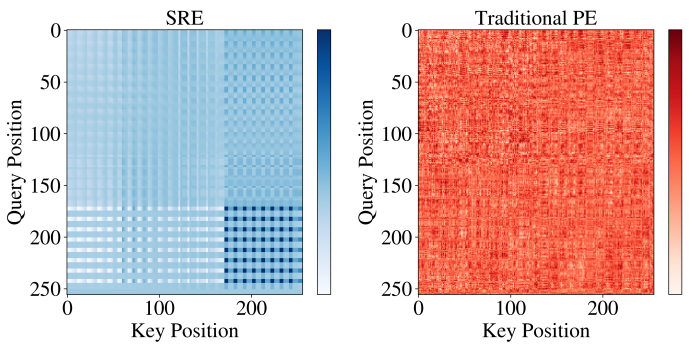


Fig. 7: Ablation on spatial relational encoding: Attention map.

on the random and mazes maps. Moreover, MAPF-World-Fast, MAPF-GPT-6M, and MAPF-GPT-85M each rank as the worst-performing baseline twice across the six map types. Notably, MAPF-World-Slow models multi-agent interactions by explicitly learning to predict other agents’ actions. In this way, our model employs a more principled coordination mechanism than the greedy, local cost based heuristics used by the MAPF-GPT family. Consequently, the performance advantage of MAPF-World-Slow widens significantly in more complex scenarios characterized by a large number of agents, realistic urban layouts, and large map size.

#### E. Ablation Studies

All ablation studies are conducted using the highest agent density for each map type listed in Table I.

*Evaluation of MAPF-World’s Thinking Capability.* To evaluate the world simulation (i.e., “thinking” or long-term planning) capability of our model, we test two work modes of MAPF-World with varied planning horizons  $H \in \{2, 3, 4, 5\}$ . The results are shown in Fig. 5. For MAPF-World-Thinking (Fig. 2c), the observations predicted in the next  $H$  steps are based solely on the single real observation before the  $H$  steps. The longer it “thinks”, the less real information it can use, and the more its performance degrades, as shown in Fig. 5a. In contrast, MAPF-World-Slow (Fig. 2b) replaces estimated actions with predicted other-agent actions for  $H$  “thinking”

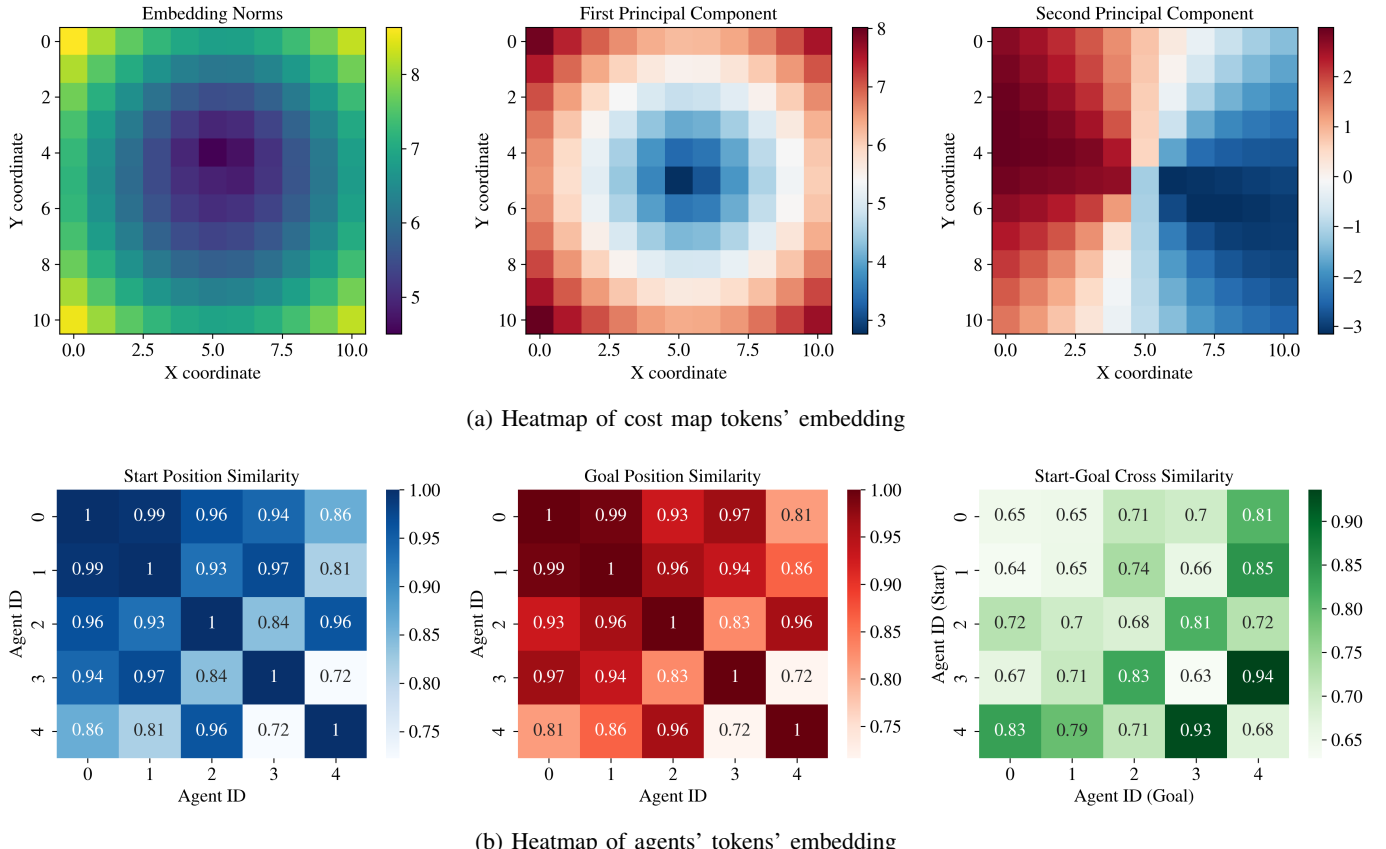


Fig. 8: Ablation on spatial relational encoding: Visualization of embeddings after SRE encoding.

steps, then uses greedy actions in the  $(H + 1)$ -th step. As shown in Fig. 5b, we found that  $H = 2$  yields the best performance. This is because greedy actions effectively guide agents toward their goals, but are suboptimal for handling complex interactions, where predicted actions perform better.

*Ablation on Spatial Relational Encoding.* We evaluate the impact of spatial relational encoding (SRE) in MAPF-World, as shown in Fig. 6. Compared to MAPF-World-Slow, removing SRE causes the performance of Slow-NSRE to drop by 3% – 19% across the six map types with an average decrease of 6.6%. This highlights the significant contribution of SRE to MAPF-World. Notably, even without SRE, Slow-NSRE still outperforms the larger model MAPF-GPT-6M, underscoring the effectiveness of the proposed MAPF-World.

We also compare the attention maps learned with SRE against those with traditional positional encoding (PE), the results are visualized in Fig. 7. The adjacent similarity of SRE is 65.38% higher than that of PE, with a distance correlation of -0.5745 and PE being 0. This indicates that SRE successfully enforces the intended spatial bias, that is, tokens corresponding to adjacent spatial locations exhibit stronger similarity, while tokens that are far apart have weaker or even negatively correlated similarity. In addition, SRE exhibits 28 distinct similarity levels, while PE only has one, which suggests that SRE captures a much richer spectrum of spatial relationships.

These results meet our design expectations and demonstrate the spatial perception ability of SRE. For more details, please refer to the appendix.

Fig. 8 further illustrates the impact of SRE by visualizing the learned embeddings. Cost map embeddings (Fig. 8a): the principal component diagram shows clear spatial patterns rather than random noise, with distinguishable regions corresponding to different features. Similarly, in the visualization of agent embeddings (Fig. 8b), it is shown that agents located closer have embeddings with higher similarity, while distant agents exhibit lower similarity. Furthermore, the cross-similarity graph reflects the encoded relationship between agents' start and target positions.

The results of ablation studies suggest that both the model's predictive planning depth and its spatial reasoning mechanism are crucial to achieving high performance.

#### F. Limitations

While MAPF-World demonstrates strong planning capabilities, its thinking capability is limited. The model cannot navigate from the start position to the goal based solely on its “dream” (predictions) without feedback from the actual environment. This limitation primarily stems from the model's egocentric frame of reference, since local observations are relative information rather than absolute positions (current

position, goal position, etc.). Long sequences of internal predictions without external grounding can lead to compounding errors. Future work could explore incorporating global context or alternative state representations.

## VI. CONCLUSION

In this work, we propose MAPF-World, an autoregressive action world model for MAPF inspired by Kahneman’s fast-slow dual system. By integrating a fast reactive policy with a slow predictive world model, MAPF-World overcomes key limitations of purely reactive policy models in partially observable multi-agent settings. Our approach achieves state-of-the-art, far-sighted planning performance with 96.5% smaller model and 92% less training data than leading baselines. We also introduce a pipeline to generate realistic benchmarks from real-world city data, addressing the critical need for MAPF solvers to generalize to practical scenarios. Experimental results indicate that the generated real-world maps present novel and demanding challenges for existing MAPF solvers. We believe MAPF-World and our real-world map generator represent significant steps toward developing more robust and generalizable solutions for MAPF.

## REFERENCES

- [1] R. Stern, N. R. Sturtevant, A. Felner, S. Koenig, H. Ma, T. T. Walker, J. Li, D. Atzmon, L. Cohen, T. K. S. Kumar, E. Boyarski, and R. Bartak, “Multi-agent pathfinding: Definitions, variants, and benchmarks,” *Symposium on Combinatorial Search (SoCS)*, pp. 151–158, 2019.
- [2] L. Sun, Y. Yang, Q. Duan, Y. Shi, C. Lyu, Y.-C. Chang, C.-T. Lin, and Y. Shen, “Multi-agent coordination across diverse applications: A survey,” *arXiv preprint arXiv:2502.14743*, 2025.
- [3] J. Yu and S. LaValle, “Structure and intractability of optimal multi-robot path planning on graphs,” in *Proceedings of the AAAI Conference on Artificial Intelligence*, vol. 27, no. 1, 2013, pp. 1443–1449.
- [4] J. Yu, “Intractability of optimal multirobot path planning on planar graphs,” *IEEE Robotics and Automation Letters*, vol. 1, no. 1, pp. 33–40, 2015.
- [5] H. Ma, C. Tovey, G. Sharon, T. Kumar, and S. Koenig, “Multi-agent path finding with payload transfers and the package-exchange robot-routing problem,” in *Proceedings of the AAAI Conference on Artificial Intelligence*, vol. 30, no. 1, 2016.
- [6] J. Banfi, N. Basilico, and F. Amigoni, “Intractability of time-optimal multirobot path planning on 2d grid graphs with holes,” *IEEE Robotics and Automation Letters*, vol. 2, no. 4, pp. 1941–1947, 2017.
- [7] G. Sharon, R. Stern, A. Felner, and N. R. Sturtevant, “Conflict-based search for optimal multi-agent pathfinding,” *Artificial intelligence*, vol. 219, pp. 40–66, 2015.
- [8] M. Liu, H. Ma, J. Li, and S. Koenig, “Task and path planning for multi-agent pickup and delivery,” in *Proceedings of the International Joint Conference on Autonomous Agents and Multiagent Systems (AAMAS)*, 2019.
- [9] K. Okumura, M. Machida, X. Défago, and Y. Tamura, “Priority inheritance with backtracking for iterative multi-agent path finding,” *Artificial Intelligence*, vol. 310, p. 103752, 2022.
- [10] K. Okumura, “Improving lacam for scalable eventually optimal multi-agent pathfinding,” in *Proceedings of the Thirty-Second International Joint Conference on Artificial Intelligence*, 2023, pp. 243–251.
- [11] ——, “Engineering lacam\*: Towards real-time, large-scale, and near-optimal multi-agent pathfinding,” *arXiv preprint arXiv:2308.04292*, 2023.
- [12] Y. Wang, B. Xiang, S. Huang, and G. Sartoretti, “Scrimp: Scalable communication for reinforcement-and imitation-learning-based multi-agent pathfinding,” in *2023 IEEE/RSJ International Conference on Intelligent Robots and Systems (IROS)*. IEEE, 2023, pp. 9301–9308.
- [13] H. Jiang, Y. Wang, R. Veerapaneni, T. Duhan, G. Sartoretti, and J. Li, “Deploying ten thousand robots: Scalable imitation learning for lifelong multi-agent path finding,” 2024.
- [14] A. Andreychuk, K. Yakovlev, A. Panov, and A. Skrynnik, “Mapf-gpt: Imitation learning for multi-agent pathfinding at scale,” in *Proceedings of the AAAI Conference on Artificial Intelligence*, vol. 39, no. 22, 2025, pp. 23 126–23 134.
- [15] ——, “Advancing learnable multi-agent pathfinding solvers with active fine-tuning,” *arXiv preprint arXiv:2506.23793*, 2025.
- [16] D. Kahneman, *Thinking, fast and slow*. macmillan, 2011.
- [17] N. Sturtevant, “Benchmarks for grid-based pathfinding,” *Transactions on Computational Intelligence and AI in Games*, vol. 4, no. 2, pp. 144 – 148, 2012. [Online]. Available: <http://web.cs.du.edu/~sturtevant/papers/benchmarks.pdf>
- [18] A. Skrynnik, A. Andreychuk, A. Borzilov, A. Chernyavskiy, K. Yakovlev, and A. Panov, “Pogema: A benchmark platform for cooperative multi-agent pathfinding,” in *The Thirteenth International Conference on Learning Representations*, 2025.
- [19] Y. Zhang, M. C. Fontaine, V. Bhatt, S. Nikolaidis, and J. Li, “Multi-robot coordination and layout design for automated warehousing,” in *Proceedings of the Thirty-Second International Joint Conference on Artificial Intelligence*, 2023, pp. 5503–5511.
- [20] Y. Zhang, M. Fontaine, V. Bhatt, S. Nikolaidis, and J. Li, “Arbitrarily scalable environment generators via neural cellular automata,” *Advances in Neural Information Processing Systems*, vol. 36, pp. 57212–57225, 2023.
- [21] C. Qian, Y. Zhang, and J. Li, “A quality diversity approach to automatically generate multi-agent path finding benchmark maps,” in *Proceedings of the International Symposium on Combinatorial Search*, vol. 17, 2024, pp. 279–280.
- [22] Z. Bnaya and A. Felner, “Conflict-oriented windowed hierarchical cooperative a,” in *2014 IEEE International Conference on Robotics and Automation (ICRA)*. IEEE, 2014, pp. 3743–3748.
- [23] Y. Wang, T. Duhan, J. Li, and G. Sartoretti, “Lns2+rl: Combining multi-agent reinforcement learning with large neighborhood search in multi-agent path finding,” in *Proceedings of the AAAI Conference on Artificial Intelligence*, vol. 39, no. 22, 2025, pp. 23 343–23 350.
- [24] D. Ha and J. Schmidhuber, “World models,” *arXiv preprint arXiv:1803.10122*, 2018.
- [25] ——, “Recurrent world models facilitate policy evolution,” *Advances in neural information processing systems*, vol. 31, 2018.
- [26] D. Hafner, T. Lillicrap, J. Ba, and M. Norouzi, “Dream to control: Learning behaviors by latent imagination,” in *International Conference on Learning Representations*, 2019.
- [27] D. Hafner, T. P. Lillicrap, M. Norouzi, and J. Ba, “Mastering atari with discrete world models,” in *International Conference on Learning Representations*, 2020.
- [28] D. Hafner, J. Pasukonis, J. Ba, and T. Lillicrap, “Mastering diverse control tasks through world models,” *Nature*, pp. 1–7, 2025.
- [29] A. Kanervisto, D. Bignell, L. Y. Wen, M. Grayson, R. Georgescu, S. Valcarcel Macua, S. Z. Tan, T. Rashid, T. Pearce, Y. Cao *et al.*, “World and human action models towards gameplay ideation,” *Nature*, vol. 638, no. 8051, pp. 656–663, 2025.
- [30] J. Ding, Y. Zhang, Y. Shang, Y. Zhang, Z. Zong, J. Feng, Y. Yuan, H. Su, N. Li, N. Sukennik *et al.*, “Understanding world or predicting future? a comprehensive survey of world models,” *ACM Computing Surveys*, 2024.
- [31] R. Bommasani, D. A. Hudson, E. Adeli, R. Altman, S. Arora, S. von Arx, M. S. Bernstein, J. Bohg, A. Bosselut, E. Brunskill *et al.*, “On the opportunities and risks of foundation models,” *arXiv preprint arXiv:2108.07258*, 2021.
- [32] J. Cen, C. Yu, H. Yuan, Y. Jiang, S. Huang, J. Guo, X. Li, Y. Song, H. Luo, F. Wang *et al.*, “Worldvla: Towards autoregressive action world model,” *arXiv preprint arXiv:2506.21539*, 2025.
- [33] Y. LeCun, “A path towards autonomous machine intelligence version 0.9. 2, 2022-06-27,” *Open Review*, vol. 62, no. 1, pp. 1–62, 2022.
- [34] H. Chen, J. Liu, C. Gu, Z. Liu, R. Zhang, X. Li, X. He, Y. Guo, C.-W. Fu, S. Zhang *et al.*, “Fast-in-slow: A dual-system foundation model unifying fast manipulation within slow reasoning,” *arXiv preprint arXiv:2506.01953*, 2025.